A structural comparison of three isoforms of anionic trypsin from chum salmon (*Oncorhynchus keta*)

Eiko Toyota,[a]* Daisuke Iyaguchi,[a] Haruo Sekizaki,[a] Midori Tateyama[b] and Kenneth K. S. Ng[c]

[a]Faculty of Pharmaceutical Sciences, Health Sciences University of Hokkaido, Japan, [b]School of Nursing and Social Services, Health Sciences University of Hokkaido, Japan, and [c]Department of Biological Sciences, University of Calgary, Canada

Correspondence e-mail: toyota@hoku-iryo-u.ac.jp

Three anionic salmon trypsin isoforms (CST-1, CST-2 and CST-3) were isolated from the pyloric caeca of chum salmon (*Oncorhynchus keta*). The order of catalytic efficiency (K_m/k_{cat}) of the isoforms during BAPA hydrolysis was CST-2 > CST-1 > CST-3. In order to find a structural rationalization for the observed difference in catalytic efficiency, the X-ray crystallographic structures of the three isoforms were compared in detail. Some structural differences were observed in the C-terminal α-helix, interdomain loop and active-site region. From the results of the detailed comparison, it appears that the structural flexibility of the C-terminal α-helix, which interacts with the N-terminal domain, and the substrate-binding pocket in CST-3 are lower than those in CST-1 and CST-2. In addition, the conformation of the catalytic triad (His57, Asp102 and Ser195) differs among the three isoforms. The imidazole N atom of His57 in CST-1 and CST-2 forms a hydrogen bond to the hydroxyl O atom of Ser195, but the distance between the imidazole N atom of His57 and the hydroxyl O atom of Ser195 in CST-3 is too great (3.8 Å) for the formation of a hydrogen bond. Thus, the nucleophilicity of the hydroxyl group of Ser195 in CST-3 is weaker than that in CST-1 or CST-2. Furthermore, the electrostatic potential of the substrate-binding pocket in CST-2 is markedly lower than those in CST-1 and CST-3 owing to the negative charges of Asp150, Asp153 and Glu221B that arise from the long-range effect. These results may explain the higher catalytic efficiency of CST-2 compared with CST-1 and CST-3.

1. Introduction

Several studies have reported the isolation and characterization of trypsins from cold-adapted fishes (Quzen *et al.*, 1996; Torrissen, 1984; Uchida *et al.*, 1984a,b; Asgeirsson *et al.*, 1989; Simpson *et al.*, 1984a,b; Genicot *et al.*, 1988; Ahsan & Watabe, 2001; Martinez *et al.*, 1988). These fish trypsins resemble mammalian trypsins in many respects but are different in others. For example, most of the fish trypsins are less stable than mammalian trypsins at acidic pH and high temperatures. Moreover, multiple isoforms of trypsin have been found in many fish species, while only one cationic and one anionic form of trypsin have been found in mammals (Figarella *et al.*, 1975; Ohlsson & Tegner, 1973; Puigserver & Desnuelle, 1971; Voytek & Gjessing, 1971). In addition, the main form of fish trypsin is anionic, while the main form of mammalian trypsin is cationic (Quzen *et al.*, 1996).

research papers

It has also been reported that enzymes from cold-adapted fishes have higher catalytic efficiencies compared with their mammalian counterparts. For example, the catalytic efficiency (K_m/k_{cat}) of anionic Atlantic salmon trypsin (AST) is about 20-fold higher at 310 K and 35-fold higher at 277 K than that of bovine trypsin (BT) (Quzen *et al.*, 1996). However, the catalytic efficiency of cationic Atlantic salmon trypsin resembles that of BT (Schrøder *et al.*, 1998). In addition, Smalås and coworkers reported structural rationalizations of the differences in catalytic efficiency and thermostability between AST and BT (Leiros *et al.*, 2000; Gorfe *et al.*, 2000; Schrøder *et al.*, 1998; Smalås *et al.*, 1994). From a detailed comparison of the X-ray crystal structures of the two trypsins, they proposed that the increased catalytic efficiency of AST is achieved owing to the lower electrostatic potential of its substrate-binding pocket, which arises from Glu221B (Gorfe *et al.*, 2000). Recently, they proved that these electrostatic interactions are one of the sources of the differences in the binding and catalytic features of AST and BT by measuring their association constants and calculating their binding free energies. For the association constants (K_a) of complexes between different P1 variants of BPTI (bovine pancreatic trypsin inhibitor) and two different trypsins (AST and BT), the K_a values for AST were 100-fold higher than the corresponding values for BT for both Lys and Arg at P1, whereas the K_a values for other P1 residues did not differ significantly between the two trypsins (Krowarsch *et al.*, 1999). Furthermore, the calculated binding free energy for benzamidine bound to AST was 3.3 kJ mol^{-1} greater than that for BT (Leiros *et al.*, 2004; Brandsdal *et al.*, 2001).

We have also studied trypsins from chum salmon (*Oncorhynchus keta*; Sekizaki, Itoh *et al.*, 2000; Sekizaki, Murakami *et al.*, 2000; Sekizaki *et al.*, 2001, 2002; Toyota *et al.*, 2002). The trypsins from chum salmon include seven anionic trypsins and one cationic trypsin. In a previous study (Toyota *et al.*, 2007), we isolated two isoforms that are present in small amounts (CST-1 and CST-2) and the main isoform (CST-3) from the pyloric caeca of chum salmon. The isoelectric points of CST-1, CST-2 and CST-3 are 5.8, 5.4 and 5.6, respectively, and thus these isoforms are anionic trypsins. The catalytic efficiencies (K_m/k_{cat}) of the three anionic chum salmon trypsins (CST-1, CST-2 and CST-3) during BAPA (benzoyl-L-arginine-*p*-nitroanilide) hydrolysis are 22-fold to 38-fold higher than that of bovine trypsin (BT) at 278–308 K. In addition, the catalytic efficiencies of CST-1 and CST-2 during BAPA hydrolysis were more efficient than that of CST-3 owing to a twofold increase in turnover (k_{cat}) and a slight decrease in K_m. In this study, in order to find a structural rationalization for the observed differences in catalytic efficiency among the three isoforms, we determined the X-ray crystallographic structures of the three isoforms (CST-1, CST-2 and CST-3). Although the crystal structure of CST-1 agreed with the structure of PDB entry 1mbq, which we previously reported as the crystal structure of CST (Toyota *et al.*, 2002), we obtained new crystal structures for CST-2 and CST-3. We describe the differences between these crystal structures that might explain their higher affinity for positively charged substrates.

Table 1
Crystallographic data and refinement statistics.

R.m.s.d., root-mean-square deviation. Values in parentheses are for the highest resolution shell.

	CST-1	CST-2	CST-3
Data-collection statistics			
Space group	$P2_12_12_1$	$P2_12_12_1$	$P2_12_12_1$
Unit-cell parameters			
a (Å)	65.0	61.3	44.3
b (Å)	80.5	75.2	47.5
c (Å)	80.8	82.0	81.5
Wavelength (Å)	1.54	1.54	1.54
Total reflections	129797	122391	188412
Unique reflections	33267	37328	27417
Resolution (Å)	50.0–1.90	50.0–1.75	50.0–1.50
	(1.97–1.90)	(1.81–1.75)	(1.55–1.50)
Completeness (%)	97.1 (96.7)	95.9 (95.7)	96.6 (93.8)
Redundancy	3.9 (3.9)	3.3 (3.2)	6.9 (6.8)
R_{merge}† (%)	0.084 (0.351)	0.060 (0.357)	0.040 (0.122)
Refinement statistics			
Resolution (Å)	20.0–1.90	20.0–1.75	20.0–1.50
R factor‡/R_{free}§ (%)	19.4/22.2	20.6/22.3	18.5/19.5
No. of amino-acid residues	440	442	221
No. of inhibitor molecules	2	2	1
No. of calcium ions	2	2	1
No. of solvent atoms	295	227	233
R.m.s.d. from ideal			
Bond lengths (Å)	0.0047	0.0049	0.0046
Bond angles (°)	1.356	1.373	1.366
Average B factor (Å^2)	17.99	23.32	17.33
Ramachandran plot (%)			
Most favoured	87.0	87.5	86.5
Additionally allowed	13.0	12.5	13.5

† $R_{merge} = \sum_{hkl} \sum_i I_i(hkl)$, where $I_i(hkl)$ is the *i*th observation of reflection *h* and $\langle I(hkl) \rangle$ is the mean intensity of all observations of reflection *hkl*. ‡ *R* factor = $\sum_{hkl} ||F_{obs}| - |F_{calc}||/\sum_{hkl} |F_{obs}|$, where $|F_{obs}|$ and $|F_{calc}|$ are observed and calculated structure-factor amplitudes. § R_{free} was calculated for a randomly selected 10% of reflections that were not used in the refinement.

2. Materials and methods

2.1. Purification and crystallization

Salmon trypsin was isolated from the pyloric caeca of chum salmon according to a previously reported procedure (Sekizaki *et al.*, 2000). Three isoforms (CST-1, CST-2 and CST-3) were obtained by DEAE anion-exchange chromatography (Toyota *et al.*, 2007). Their nucleotide sequences were determined using cDNA clones (Toyota *et al.*, 2002). The cocrystallization of trypsin–benzamidine complexes was performed by the hanging-drop vapour-diffusion method at room temperature. The crystals of CST-1 and CST-3 were obtained by equilibrating droplets containing 0.3 m*M* trypsin, 200 m*M* MgSO$_4$, 1 m*M* CaCl$_2$, 3 m*M* benzamidine and 50 m*M* Tris–HCl buffer pH 8.1 against a reservoir solution containing 0.8 *M* MgSO$_4$ and 100 m*M* Tris–HCl buffer pH 8.5. The crystal of CST-2 was obtained from 0.1 *M* Na HEPES buffer pH 7.5, 17% PEG 4000 and 10% 2-propanol.

2.2. Crystallographic data collection and structural refinements

Complete X-ray diffraction data for CST-1, CST-2 and CST-3 were collected to 1.90, 1.75 and 1.50 Å resolution, respectively, using an R-AXIS IV^{++} image-plate detector. The diffraction experiments were performed under cryocooling

conditions (100 K) after the crystals had been soaked in cryoprotectant consisting of 20% glycerol for CST-1 and CST-3 and 15% glycerol for CST-2 in the reservoir solution. The diffraction images were analyzed and processed using the program *HKL*-2000 (Otwinowski & Minor, 1997). The crystals of CST-1, CST-2 and CST-3 belonged to space group $P2_12_12_1$. The unit-cell parameters for CST-1, CST-2 and CST-3 are given in Table 1. These parameters indicated the presence of two molecules per asymmetric unit for CST-1 and CST-2 and one molecule per asymmetric unit for CST-3, with V_M values of 2.20, 1.97 and 1.79 $Å^3\,Da^{-1}$, respectively, based on an estimated molecular mass of 24 kDa (Matthews, 1968). The data-collection statistics are summarized in Table 1.

The structures of CST-1, CST-2 and CST-3 were determined by the molecular-replacement method with the program *AMoRe* (Navaza, 1994) in the resolution range 20.0–3.0 Å using the crystal structure of PDB entry 1mbq as a search model (Toyota *et al.*, 2002). The final models were obtained by refinement using the program *CNS* (Brünger *et al.*, 1998) with manual model modifications made using the program *O* (Jones *et al.*, 1991). The refined models of CST-1, CST-2 and CST-3 contained 220, 221 and 221 amino-acid residues, respectively. Two residues in the C-terminus of CST-1 were not visible, indicating that they had been deleted. In contrast, electron densities for the C-terminus were detected in the structures of CST-2 and CST-3, indicating that the two residues had not been deleted, although the extreme C-terminal residues could not be modelled because of their poor electron densities. An analysis of protein geometry was performed using the program *PROCHECK* (Laskowski *et al.*, 1993). The final refinement statistics are given in Table 1.

3. Results

3.1. Sequence and overall crystal structure

Sequence work indicated that the chum salmon trypsin gene is comprised of 222 residues. There are five sequence differences between CST-1 and CST-2 (at residues 64, 152, 153, 244 and 245), four sequence differences between CST-1 and CST-3 (at residues 61, 236, 244 and 245) and five sequence differences between CST-2 and CST-3 (at residues 61, 64, 152, 153 and 236). The net charge is −3 for CST-1 (4 Arg, 9 Lys, 7 Asp, 9 Glu), −4 for CST-2 (4 Arg, 8 Lys, 8 Asp, 8 Glu) and −2 for CST-3 (4 Arg, 9 Lys, 6 Asp, 9 Glu).

The crystal structures of CST-1, CST-2 and CST-3 were solved by the molecular-replacement method using the structure of PDB entry 1mbq, which we previously reported as the crystal structure of chum salmon trypsin (Toyota *et al.*, 2002), as a model. The electron density of the three isoforms was well defined for both the trypsin and benzamidine parts of the complex. The refined model of CST-1 is in good agreement with 1mbq, but the crystal packing is different. CST-1 is comprised of 220 amino-acid residues, *i.e.* the last two residues (Thr244 and Tyr245) at the C-terminus have been deleted. In contrast, the main chain of the CST-2 and CST-3 isoforms can be traced with continuous density from the N-terminus to

residue 222, but has a poor electron-density map for the last residue (Tyr245). Thus, CST-2 and CST-3 are comprised of 222 residues, two more residues than CST-1.

A superimposition of the main-chain atoms of the three isoforms is shown in Fig. 1. The r.m.s. deviations for the main-chain atoms between CST-1 and CST-2, between CST-2 and CST-3 and between CST-3 and CST-1 are 0.26, 0.27 and 0.25 Å, respectively.

Fig. 2(*a*) shows the distances between C^α atoms between CST-1 and CST-2, between CST-2 and CST-3 and between CST-3 and CST-1. The values reveal the regions that are structurally different between the isoforms. The largest structural differences between the isoforms are found at residues 146–152 (described as an autolysis loop in bovine trypsin) and residues 235–245 of the C-terminal α-helix. This difference is probably explained by their respective structural flexibilities and also by the different sequences in both regions, *i.e.* Lys152 in CST-1 and CST-3 is changed to Gly in CST-2 and Asn153 in CST-1 and CST-3 is changed to Asp in CST-2. In the C-terminal α-helix, the extreme C-terminal residue of CST-1 is Ala243, whereas it is Tyr245 in both CST-2 and CST-3; Asp236 in CST-1 and CST-2 is changed to Asn in CST-3. Larger differences are found in the regions containing residues 34–38, 95–101, 115–118, 124–128 and 200–202; these residues are conserved in all isoforms.

Fig. 2(*b*) shows a comparison of temperature factors between the three isoforms. The temperature factors of C^α atoms are plotted as the difference from the average value for each isoform. These plots reveal the relatively flexible regions of the structures for each individual isoform. The variations in the plots are similar between the three isoforms across the
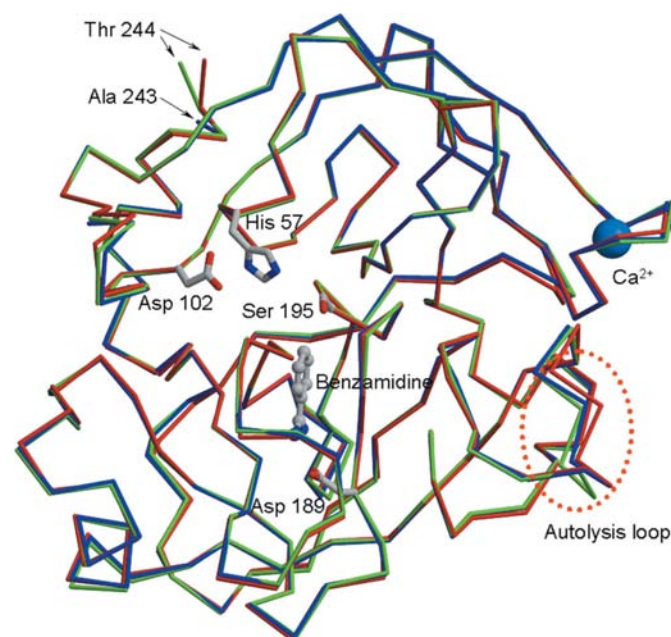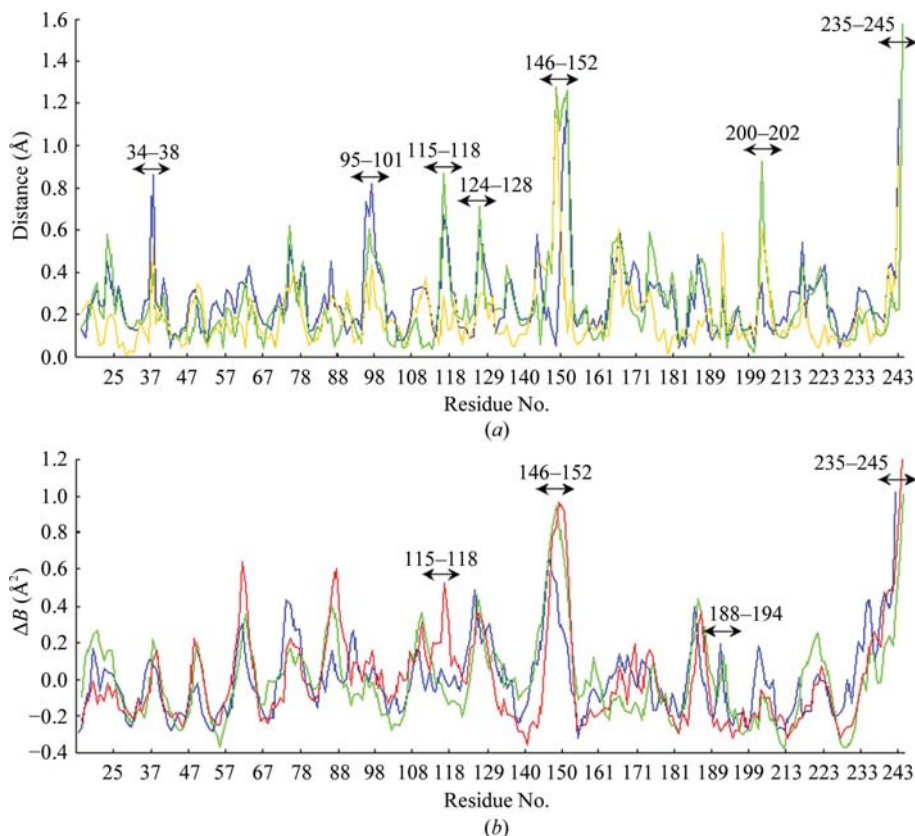

Figure 1
Superimposition of the C^α atoms in CST-1, CST-2 and CST-3. The C^α traces of CST-1, CST-2 and CST-3 are shown in blue, green and red, respectively. The three catalytic residues (Asp102, His57 and Ser195), benzamidine and calcium ions are included. The autolysis loop is shown as a red dashed circle.

entire sequence, but there are some marked differences in the regions containing residues 115–118 of the interdomain loop, 146–152 of the autolysis loop, 188–194 of the active site and 235–245 of the C-terminal α-helix.

3.2. The C-terminal α-helix

Residues 231–245 (the C-terminal α-helix and preceding residues) display gradually increasing temperature factors along the chain, as shown in Fig. 2(b). The interactions in this

Figure 2
A comparison of the structure and temperature factors of three isozymes. (a) The distance values for Cα atoms between CST-1, CST-2 and CST-3 were calculated from the superimposed model for each residue. The distances between CST-1 and CST-2 (yellow), between CST-2 and CST-3 (green) and between CST-3 and CST-1 (blue) are plotted for each residue along the chain. (b) $\Delta B = B_i - B_{ave}/B_{ave}$, where B_i is the B-factor value of the Cα atoms of each residue and B_{ave} is the average value of B_i. The values for CST-1, CST-2 and CST-3 are shown in blue, green and red, respectively.
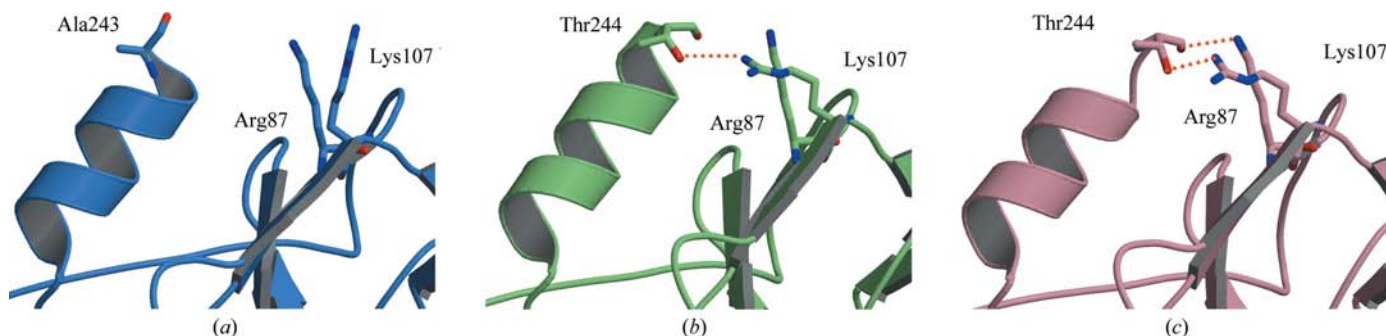
region are shown in Fig. 3. It is well known that the C-terminal α-helix in BT is stabilized by ion-pair interactions between the carboxyl group of the extreme C-terminal residue Asn245 and the N atoms of the two positively charged residues Lys87 and Lys107 (Bartunik et al., 1989). In CST-1, however, the Ala243 residue located at the extremity of the C-terminus is unable to form this interaction, since the distances between the carboxyl O atoms of Ala243 and the N atoms of Arg87 (Lys in BT) and Lys107 are too great (6.9 and 6.1 Å, respectively; Fig. 3a). In contrast, the extreme C-terminal residue of both CST-2 and CST-3 is Tyr245, although this residue could not be modelled because of its poor electron density. The carboxyl group of Tyr245 is prevented from interacting with the adjacent residues owing to the large and bulky side chain. As expected, the carboxyl group of Tyr245 in CST-2 and CST-3 does not form any interactions with adjacent residues. Instead, the hydroxyl O atom of the side chain and the carbonyl O atom of the main chain of Thr244 in CST-3 form hydrogen bonds to Arg87 (3.08 Å) and Lys107 (3.29 Å), respectively (Fig. 3c). In contrast, the interactions of Thr244 with Arg87 and Lys107 in CST-2 are very weak (3.81 and 4.98 Å, respectively; Fig. 3b). Thus, the interaction of the C-terminal α-helix in CST-3 with the N-terminal domain is stable and the flexibility of the N- and C-terminal domains is reduced. It is possible that these structural features related to domain flexibility generate the observed differences in enzymatic activity.

3.3. The autolysis loop

It is well known that the loop from residue 142 to 153 in BT, which is called the 'autolysis loop', is more flexible than

Figure 3
A comparison of the interactions of the C-terminal α-helix with the N-terminal domain between the three isozymes. The interactions of the extremity of the C-terminal α-helix with the N-terminal domain are shown for CST-1 (a), CST-2 (b) and CST-3 (c). The red dashed lines indicate hydrogen bonds. Residue numbers are labelled.

Table 2
Comparison of hydrogen bonds and other nonbonded distances in the active-site region for chum salmon trypsin isoforms (CST-1, CST-2 and CST-3), Atlantic salmon trypsin (AST) and bovine trypsin (BT).

Bond	Distance (Å)				
	CST-1	CST-2	CST-3	AST†	BT‡
His57 N$^{\delta 1}$—Asp102 O$^{\delta 2}$	2.7	2.6	2.8	2.7	2.7
His57 N$^{\varepsilon 2}$—Ser195 O$^{\gamma}$	3.2	3.0	3.8	3.2	3.0
His57 N$^{\varepsilon 2}$—water1	—	3.3	2.9	—	—
Asp189 O$^{\delta 2}$—Ala221 N	3.1	3.1	3.0	2.9	2.8
Asp189 O$^{\delta 1}$—Ser190 N	2.7	2.7	2.7	2.9	2.9
Asp189 O$^{\delta 1}$—BEN§ N2	2.9	2.8	2.8	2.8	2.9
Asp189 O$^{\delta 2}$—BEN N1	2.8	2.8	2.8	2.7	2.9
Ser195 O$^{\gamma}$—water1	—	3.2	2.7	—	—
BEN N2—Ser190 O$^{\gamma}$	2.9	2.7	2.9	3.1	3.0
BEN N1—Gly219 O	2.9	3.0	2.9	2.9	2.9

† PDB code 2tbs.   ‡ PDB code 1bty.   § Benzamidine.
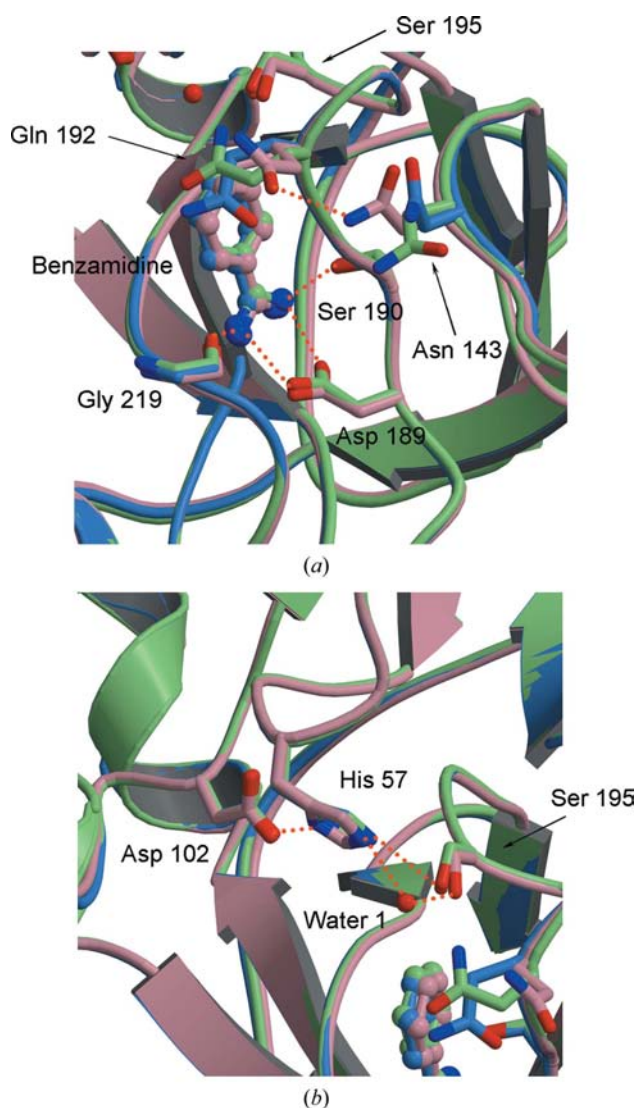
Figure 4
A detailed view of the active site. Interactions between benzamidine, active residues and residues located in the substrate-binding pocket are shown. The red dashed lines indicate hydrogen bonds. CST-1, CST-2 and CST-3 are shown in blue, green and pink, respectively.

other regions (Bartunik *et al.*, 1989) since bovine β-trypsin autolysis at Lys145-Ser146 leads to the formation of α-trypsin and autolysis at Lys188-Asp189 leads to the formation of ψ-trypsin (Fehlhammer & Bode, 1975). The temperature factors of this region in salmon trypsins are considerably higher than the average. However, the electron-density maps of this region are better defined in salmon trypsins than in BT. When the amino-acid sequences of the salmon trypsin isoforms were compared with those of BT, Tyr151 in BT was found to be deleted in salmon trypsin. The role of Tyr151 is unclear, but the lack of a large and bulky Tyr residue may participate in the stabilization of the autolysis loop in salmon trypsin. Residue 145 in salmon trypsin is a methionine; thus, it is not a site of autolysis. Although sequence differences between the three isoforms were found at residues 152 (Lys in CST-1 and CST-3, Gly in CST-2) and 153 (Asn in CST-1 and CST-3, Asp in CST-2), no structural differences were found between the isoforms.

3.4. The active-site and specificity-pocket region

Figs. 4(*a*) and 4(*b*) show a superimposition of the benzamidine molecule, the substrate-binding residue (Asp189), the catalytic triad (His57, Asp102 and Ser195) and the walls of the specificity pocket in the three salmon trypsin isoforms. The main hydrogen-bond distances in this region are listed in Table 2. The amidinium group (N1, N2) of the benzamidine inhibitor forms salt bridges with the carboxylate O atoms of Asp189 in all isoforms. The N1 and N2 atoms also donate hydrogen bonds to the carbonyl O atom of Gly219 and the hydroxyl O atom of Ser190, respectively. In addition, the carboxylate O atoms of Asp189 accept hydrogen bonds from the amide N atom of Ala221 and Ser190. In a comparison among the three isoforms, the most significant difference was found for Gln192. The side chain of Gln192 in CST-3 forms a hydrogen bond to the side chain of Asn143 in the autolysis loop, whereas Gln192 in CST-1 and CST-2 is unable to form this interaction. This behaviour is supported by the temperature-factor data. The temperature factor in the region containing Glu192 (residues 188–194) is increased in CST-1 and CST-2, but that in CST-3 does not vary, as is shown in Fig. 2(*b*). This result suggests that the structures of the substrate-binding sites in CST-1 and CST-2 are more flexible than that in CST-3.

The conformations of the catalytic triad (His57, Asp102 and Ser195) are slightly different compared with those of the three isoforms, as is shown in Fig. 4(*b*). The amide N atom of His57 forms a strong hydrogen bond to the carboxylate O atom of Asp102 in the three isoforms (2.7–2.8 Å). The imidazole N atom of His57 in CST-1 and CST-2 also forms a hydrogen bond to the hydroxyl O atom of Ser195, but the distance between His57 and Ser195 in CST-3 is too great (3.8 Å) for the formation of a hydrogen bond. Instead, the imidazole N atom of His57 in CST-3 forms a water-mediated hydrogen bond to the hydroxyl O atom of Ser195. Thus, the nucleophilicity of the Ser195 hydroxyl group in CST-3 is weaker than that in CST-1 or CST-2.

3.5. The interdomain loop

The interdomain loop (residues 109–132) is a long loop that links the N- and C-terminal domains and is located close to the catalytic residues. The amino-acid sequence of this loop is completely conserved in the three isoforms, despite the fact that the main-chain structure differs between the three isoforms in this loop region. In Fig. 2(a), differences in main-chain structure between CST-1 and CST-2 can hardly be seen in the interdomain loop, but those between CST-1 and CST-3 and between CST-2 and CST-3 are obvious at residues 115–118 and 124–128. Furthermore, the temperature factor of residues 115–118 is only increased in CST-3. These results indicate that the main-chain conformations of residues 115–118 and 124–128 in CST-3 are different from those in CST-1 and CST-2 and that the double-domain structure of CST-3 may be looser than those in CST-1 and CST-2.

4. Discussion

In our previous paper (Toyota *et al.*, 2007), the K_m values of CST-1 and CST-2 during BAPA hydrolysis were found to be slightly higher than that of CST-3, which is the main isoform. The k_{cat} values for CST-1 and CST-2 were about twice as high as that of CST-3. Consequently, the catalytic efficiencies (K_m/k_{cat}) of CST-1 and CST-2 were more efficient than that of CST-3. In order to understand how small differences in sequence and structure may be responsible for significant changes in enzymatic activity, we analyzed the X-ray crystal structures of the three isoforms. As a result, it appeared that the flexibility of the C-terminal α-helix in CST-1 and CST-2 was greater than that in CST-3. Furthermore, the structures of the active-site and specificity-pocket region in CST-1 and CST-2 are more flexible than those of CST-3. Thus, their flexible structure is one of the reasons for the increased catalytic efficiency of CST-1 and CST-2 compared with CST-3, *i.e.* since the flexibility of the substrate-binding pocket in CST-3 is lower than that of the other isoforms, hydrolysis products will find it harder to leave the pocket and as a result the k_{cat} values of CST-3 are lower than those of CST-1 and CST-2.

The catalytic triad residues (Asp102, His57 and Ser195) are sited at the junction between the C-terminal domain and N-terminal domain and the imidazole ring of the His57 forms hydrogen bonds to the side chains of Asp102 and Ser195. The catalytic power of serine proteases involves nucleophilic addition of the hydroxyl group of Ser195 to the carbonyl C atom of the substrate (Bender & Kézdy, 1964). Generation of the effective nucleophile is accomplished by the transfer of a proton from the hydroxyl group of Ser195 to the imidazole of His57 and therefore the role of Asp102 requires its precise positioning in the active site and its negatively charged state under the conditions of the reaction (Kossiakoff & Spencer, 1981). The catalytic effectiveness of the Asp102-His57-Ser195 triad does not arise from a chemical effect perpetuated through a hydrogen-bonding system as proposed in the charge-relay and the double proton-transfer mechanisms, but

is rather a function of the standard chemical characteristics of these groups made maximally effective and efficient by their precise stereochemical positioning in the enzyme–substrate complex (Kossiakoff & Spencer, 1981). As shown in Fig. 4(b), the conformations of Asp102-His57-Ser195 in the three isoforms are slightly different. The distance between the imidazole N atom of His57 and the hydroxyl O atom of Ser195 in CST-3 is too great (3.8 Å) to form a hydrogen bond, whereas the distances between the two atoms in CST-1 and CST-2 are 3.2 and 3.0 Å, respectively (Table 2). Thus, the nucleophilicity of the Ser195 hydroxyl in CST-3 is weaker than that in CST-1 or CST-2 and as a result CST-3 is less catalytically efficient during BAPA hydrolysis than CST-1 and CST-2. This may be the most significant factor in the higher catalytic efficiencies of CST-1 and CST-2 compared with CST-3. The catalytic efficiencies (K_m/k_{cat}) of the chum salmon trypsin isoforms (CST-1, CST-2 and CST-3) in this study during BAPA hydrolysis were 20-fold more efficient than that of bovine trypsin (BT) at 308 K and their enzyme activity increased more at low temperatures (298–278 K; Toyota *et al.*, 2007). The catalytic efficiency of anionic Atlantic salmon trypsin (AST) is also about 20-fold higher than BT at 310 K and 35-fold higher at 277 K (Quzen *et al.*, 1996). The increased catalytic efficiency seems to arise from a combination of a markedly reduced K_m and an increased k_{cat}. According to the standard serine proteinase mechanism, the rate-determining step in amide hydrolysis is the acylation process (Zerner & Bender, 1964). The K_m and k_{cat} values should therefore approximate the true binding affinity (K_s) and acylation rate (k_2). Thus, the increased catalytic efficiency of CST and AST is related to their higher substrate-binding affinity.

Smalås and coworkers reported structural rationalizations of the differences in catalytic efficiency between mammalian and cold-adapted fish trypsins. From a comparison of X-ray crystal structures, they proposed that the increased substrate affinity of AST is probably achieved by a lower electrostatic potential of the substrate-binding pocket arising from Glu221B and from the lack of five hydrogen bonds adjacent to the catalytic triad (Leiros *et al.*, 2000). In addition, they reported that in measurements of complexes between different P1 variants of BPTI (bovine pancreatic trypsin inhibitor) and two different trypsins (AST and BT), the K_a values for AST were 100-fold higher than the corresponding values for BT for both Lys and Arg at P1, whereas the K_a values for other P1 residues did not differ significantly between the two trypsins (Krowarsch *et al.*, 1999). Furthermore, they calculated binding free energies for benzamidine bound to trypsin (AST and BT) as well as for binding substrate analogues (BPTI) by means of comparative MD simulations using the linear interaction energy (LIE) approach (Leiros *et al.*, 2004; Brandsdal *et al.*, 2001). Their results show that AST binds to benzamidine inhibitors 3.3 kJ mol^{-1} more strongly than BT. This is primarily caused by the negative charges of Asp150 (Ser in BT) and Glu221B that arise from the long-range effect.

There are only four amino-acid sequence differences (at positions 28, 125, 152 and 244) between CST-1 and AST and

six differences (at positions 28, 61, 125, 152, 236 and 244) between CST-3 and AST. Residue 152 is Lys in CST-1 and CST-3 but is Ser in AST; thus, the electrostatic potential of the S1 site in CST-1 and CST-3 is slightly altered. In contrast, there are five differences (at positions 28, 125, 152, 153 and 244) in the amino-acid sequences of CST-2 and AST. Residue 153 is Asp in CST-2 but Asn in AST as well as in CST-1 and CST-3. As a result, the electrostatic potential of the substrate-binding pocket in CST-2 is lower than that in AST, CST-1 and CST-3, which is caused by the negative charges of Asp150, Asp153 and Glu221B, which arise from the long-range effect. This result may be the most important reason for the higher catalytic efficiency of CST-2 compared with those of CST-1 and CST-3. Our new results help to explain how small differences in sequence and structure allow enzymes to perform their biological functions in a wide range of environments.

References

Ahsan, M. N. & Watabe, S. (2001). *J. Protein Chem.* **20**, 49–58.

Asgeirsson, B., Fox, J. W. & Bjarnason, J. B. (1989). *Eur. J. Biochem.* **180**, 85–94.

Bartunik, H. D., Summers, L. J. & Bartsch, H. H. (1989). *J. Mol. Biol.* **210**, 813–828.

Bender, M. L. & Kézdy, F. J. (1964). *J. Am. Chem. Soc.* **86**, 3704–3714.

Brandsdal, B. O., Smalås, A. O. & Åqvist, S. J. (2001). *FEBS Lett.* **499**, 171–175.

Brünger, A. T., Adams, P. D., Clore, G. M., DeLano, W. L., Gros, P., Grosse-Kunstleve, R. W., Jiang, J.-S., Kuszewski, J., Nilges, M., Pannu, N. S., Read, R. J., Rice, L. M., Simonson, T. & Warren, G. L. (1998). *Acta Cryst.* D**54**, 905–921.

Fehlhammer, H. & Bode, W. (1975). *J. Mol. Biol.* **98**, 683–692.

Figarella, C., Negri, G. A. & Guy, O. (1975). *Eur. J. Biochem.* **53**, 457–463.

Genicot, S., Feller, G. & Gerday, C. (1988). *Comp. Biochem. Physiol. B*, **90**, 601–609.

Gorfe, A. A., Brandsdal, B. O., Leiros, H.-K. S., Helland, R. & Smalås, A. O. (2000). *Proteins*, **40**, 207–217.

Kossiakoff, A. A. & Spencer, S. A. (1981). *Biochemistry*, **20**, 6462–6474.

Jones, T. A., Zou, J.-Y., Cowan, S. W. & Kjeldgaard, M. (1991). *Acta Cryst.* A**47**, 110–119.

Krowarsch, D., Dadlez, M., Buczek, O., Krokoszynska, I., Smalås, A. O. & Otlewski, J. (1999). *J. Mol. Biol.* **289**, 175–186.

Laskowski, R. A., MacArthur, M. W., Moss, D. S. & Thornton, J. M. (1993). *J. Appl. Cryst.* **26**, 283–291.

Leiros, H.-K. S., Brandsdal, B. O., Andersen, O. A., Leiros, I., Helland, R., Otlewski, J., Willassen, N. P. & Smalås, A. O. (2004). *Protein Sci.* **13**, 1056–1070.

Leiros, H.-K. S., Willassen, N. P. & Smalås, A. O. (2000). *Eur. J. Biochem.* **267**, 1039–1049.

Martinez, A., Olsen, R. L. & Serra, J. L. (1988). *Comp. Biochem. Physiol. B*, **91**, 677–684.

Matthews, B. W. (1968). *J. Mol. Biol.* **33**, 491–497.

Navaza, J. (1994). *Acta Cryst.* A**50**, 157–163.

Ohlsson, K. & Tegner, H. (1973). *Biochim. Biophys. Acta*, **317**, 328–337.

Otwinowski, Z. & Minor, W. (1997). *Methods Enzymol.* **276**, 307–326.

Puigserver, A. & Desnuelle, P. (1971). *Biochim. Biophys. Acta*, **236**, 499–502.

Quzen, H., Berglund, G. I., Smalås, A. O. & Willassen, N. P. (1996). *Comp. Biochem. Physiol. B*, **115**, 33–45.

Schrøder, H. K., Willassen, N. P. & Smalås, A. O. (1998). *Acta Cryst.* D**54**, 780–798.

Sekizaki, H., Itoh, K., Murakami, M., Toyota, E., Tanizawa, K. (2000). *Comp. Biochem. Physiol. B*, **127**, 337–346.

Sekizaki, H., Itoh, K., Toyota, E. & Tanizawa, K. (2001). *Amino Acids*, **21**, 175–184.

Sekizaki, H., Itoh, K., Toyota, E. & Tanizawa, K. (2002). *Pept. Sci.* **8**, 521–528.

Sekizaki, H., Murakami, M., Itoh, K., Toyota, E. & Tanizawa, K. (2000). *J. Mol. Catal. B Enzym.* **11**, 23–28.

Simpson, B. K. & Haard, N. F. (1984a). *Can. J. Biochem. Cell Biol.* **62**, 894–900.

Simpson, B. K. & Haard, N. F. (1984b). *Comp. Biochem. Physiol. B*, **79**, 613–622.

Smalås, A. O., Heimstad, E. S., Hordvik, A., Willassen, N. P. & Male, R. (1994). *Proteins*, **20**, 149–166.

Torrissen, K. R. (1984). *Comp. Biochem. Physiol. B*, **77**, 669–674.

Toyota, E., Iyaguchi, D., Sekizaki, H., Itoh, K. & Tanizawa, K. (2007). *Biol. Pharm. Bull.* **30**, 1648–1652.

Toyota, E., Ng, K. K. S., Kuninaga, S., Sekizaki, H., Itho, K., Tanizawa, K. & James, M. N. G. (2002). *J. Mol. Biol.* **324**, 391–397.

Uchida, N., Tsukayama, K. & Nishide, E. (1984a). *Bull. Jpn. Soc. Sci. Fish.* **50**, 129–138.

Uchida, N., Tsukayama, K. & Nishide, E. (1984b). *Bull. Jpn. Soc. Sci. Fish.* **50**, 313–321.

Voytek, P. & Gjessing, E. C. (1971). *J. Biol. Chem.* **246**, 508–516.

Zerner, B. & Bender, M. L. (1964). *J. Am. Chem. Soc.* **86**, 3669–3674.